2021 43rd Annual International Conference of the
IEEE Engineering in Medicine & Biology Society (EMBC)
Oct 31 - Nov 4, 2021. Virtual Conference

State Space Embedding of Atrial Electrograms to Detect Repetitive Conduction Patterns During Atrial Fibrillation

Ozan Özgül[1], Bart Maesen[3], Ulrich Schotten[1], Pietro Bonizzi[2], Stef Zeemering[1]

Abstract— **Repetitive atrial conduction patterns are often observed during human atrial fibrillation (AF). Repetitive patterns may be associated with AF drivers such as focal and micro-reentrant mechanisms. Therefore, tools for repetitive activity detection are of great interest as they may allow to identify the leading electrophysiological AF mechanism in an individual patient. Recurrence plots (RP) are efficient tools for repetitive activity visualization. Construction of an RP requires embedding of epicardial atrial electrograms into a phase space. In this study, we compared the conventional Takens' embedding approach and three novel approaches based on $a\ priori$ AF cycle length (AFCL) information. Approaches were benchmarked based on the similarity of the RPs they produce with a previously proposed technique, the sensitivity and specificity to detect the repetitive patterns, as well as the capability to estimate overall repetitive pattern prevalence. All techniques were applied to high-density epicardial direct contact mapping recordings in AF patients with paroxysmal AF (n=12) and persistent AF (n=9). Compared to a reference method the proposed novel techniques achieved significantly higher similarity and sensitivity values ($p<0.01$) than conventional embedding, in both paroxysmal and persistent patients. Moreover, estimated prevalences were robust against the various degrees of AF complexity present in the recordings.**

Clinical relevance— **This study presents three novel approaches for detection of repetitive patterns of conduction during AF in atrial direct contact recordings, which may aid in the identification of the leading AF mechanism in an individual patient.**

I. INTRODUCTION

During atrial fibrillation (AF), regular atrial electrical propagation originating from the sinus node is disrupted by arrhythmogenic mechanisms stemming from alternative sites in the atria. In the initial phase of the disease, the majority of these drivers are located in pulmonary veins. Therefore, electrical isolation of pulmonary veins is an efficient treatment option in this phase. The efficacy of this procedure, however, decreases in patients with more persistent forms of AF [1]. This necessitates development of computational tools for the detection of additional sources for AF. One class of potential sources are repetitive local AF drivers such as focal and micro re-entrant sources [2][3]. Independent of the type of source, these mechanisms dictate the conduction characteristics in their surroundings, which therefore may show a specific repetitive conduction pattern for a number of consecutive AF cycles. Techniques that can pinpoint atrial locations that exhibit repetitive activity and that can characterize the local conduction pattern may be instrumental in locating additional drivers of AF outside of the pulmonary veins.

Recurrence plots (RP) provide a systematic way to visualize and quantify repetitive behavior of a dynamical system through analyzing the system's trajectory in phase space [4]. The phase space trajectory of an electrogram is obtained through an embedding process which can be achieved in many different ways. In a recent work [5], we utilized local activation time information from epicardial electrodes to generate RPs for the detection of repetitive patterns during AF. Briefly, a RP was generated using an embedding over space, rather than time, such that each embedding vector consisted of the activation-phase information from all electrodes at a specific time instant. While effectively describing the underlying spatiotemporal structure and enabling a robust detection of repetitive patterns in the high-density mapping of AF, this approach relies on stable electrode positioning and exhibits inherent ambiguity associated with local activation time annotation in complex fractionated electrograms. Therefore, there is a need to develop electrogram embedding techniques that provide similar performance with respect to pattern detection while being more robust against varying electrode positioning to enable real-time application of this technique in a clinical setting. These techniques can also make ground in non-invasive recordings and contribute patient stratification and treatment selection.

This study proposes multiple electrogram embedding and RP construction strategies which can reveal spatiotemporal repetitive patterns during AF. The proposed methods generate a RP directly from the electrograms, avoiding the computation of activation-phase information. We investigated the ability of the proposed techniques to detect time intervals with repetitive atrial activation patterns. Performance was compared to the reference method as described in [5]. Furthermore, we analyzed if and how different AF complexity levels (namely paroxysmal and persistent AF) affected performance.

* This work was supported by PersonalizeAF project. This project has received funding from the European Union's Horizon 2020 research and innovation programme under the Marie Skłodowska-Curie grant agreement No 860974.

* This publication reflects only the author's view and the Agency is not responsible for any use that maybe made of the information it contains.

[1]Ozan Özgül, Stef Zeemering and Ulrich Schotten are with the Department of Physiology, CARIM, Maastricht University, Maastricht, The Netherlands o.ozgul@maastrichtuniversity.nl

[2]Pietro Bonizzi is with the Department of Data Science and Knowledge Engineering, Maastricht University, Maastricht, The Netherlands.

[3]Bart Maesen is with the Cardio-thoracic Surgery, Maastricht University Medical Centre and CARIM, Maastricht University, Maastricht, The Netherlands.

II. MATERIALS AND METHODS

A. High-density contact mapping

High-density contact mapping of AF was performed using a 16×16 grid of electrodes with 1.5 mm electrode distance in 21 patients during open-chest cardiac surgery. Epicardial unipolar electrograms were recorded from right atrial free wall and posterior left atrium with a sampling frequency of 1039 Hz. Patients were in paroxysmal AF (pAF, n=12) or persistent AF (persAF, n=9) at the time of recording.

Ventricular far-fields were removed from electrograms using Principal Component Analysis (PCA) on single ventricular beats (over all electrodes), under the assumption that the first principal component represented the ventricular contribution. Consequently, electrograms were subjected to: Band-pass filtering (40-250 Hz), rectification and low-pass filtering (20Hz) in order to highlight atrial deflection-related parts of signals [6].

B. Recurrence Plot Construction

Phase space representation of a signal $x(t)$ at t=i can be reconstructed using Takens's Theorem:

$$\vec{x}(i) = [x(i), x(i+\tau), ..., x(i+\tau(m-1)))]^T, \quad (1)$$

with m the embedding dimension - dimensionality of the phase space trajectory- and τ the time delay embedding. Recurrence $R_{i,j}$ between two time points $\vec{x}(i)$ and $\vec{x}(j)$ in the phase space occurs when the distance between these points is smaller than a threshold ϵ:

$$R_{i,j} = \mathcal{H}(\varepsilon - D(\vec{x}(i), \vec{x}(j))), \quad (2)$$

with $\mathcal{H}$ the Heaviside step function, ϵ the threshold and D the distance function. A RP is a square symmetric matrix which exhibits recurrences between all time points i, j. In this paper, we utilized the conventional approach of Takens' and three novel methods for RP generation:

1) Takens' Embedding: For each time point t, electrograms on each of N electrodes were embedded individually using (1). The resulting electrode-wise embeddings were concatenated to yield the overall embedding vector:

$$\vec{x}(i) = [\vec{x_1}(i), \vec{x_2}(i), ..., \vec{x_N}(i)], \quad (3)$$

with N the number of electrodes. Embedding parameters, m and τ were estimated by the False Nearest Neighbour Test and Average Mutual Information [7]. These parameters were calculated for each electrode and then averaged. Euclidean distances were used to construct the distance matrix.

2) Spatiotemporal Slicing: Embedding dimension m was chosen as the estimated AF cycle length (AFCL) in samples, derived from the average dominant frequency (DF) of the electrograms of all N electrodes. Time delay τ was set to 1 sample (≈1 ms). A state matrix (instead of a standard state vector) can then be generated for a sample i by taking m samples from all N electrodes, as indicated in (4):

$$S_i = \begin{bmatrix} x_1(i) & x_2(i) & \cdots & x_N(i) \\ x_1(i+1) & x_2(i+1) & \cdots & x_N(i+1) \\ \vdots & \vdots & \ddots & \vdots \\ x_1(i+(m-1)) & x_2(i+(m-1)) & \cdots & x_N(i+(m-1)) \end{bmatrix}^T, \quad (4)$$

Based on this state matrix structure, three different approaches were proposed:

a) Frobenius Norm of Spatiotemporal Slice Difference Matrices (FD-STS): The distance between two time points i, j was denoted by $D_{i,j}$ and calculated as the Frobenius norm of the difference between associated state matrices:

$$D_{i,j} = ||S_i - S_j||_F, \quad (5)$$

b) Spatiotemporal Slices of Principal Components (PCA-STS): PCA of each state matrix was computed by singular value decomposition (SVD):

$$S_i = U\Sigma V^T, \quad (6)$$

Columns of matrix V in (6) contain principal components (PC) ordered by decreasing importance. The distance between two points i, j was then estimated by weighted average of distances of their first M PCs:

$$D_{i,j} = \frac{1}{M}\sum_{k=1}^{M} w_k D(\vec{v_k}(i), \vec{v_k}(j)), \quad (7)$$

in which $\vec{v_k}(i)$ is the k^{th} PC of S_i and w_k is the weight associated with the k^{th} PC. The weight, w_k was chosen as the fraction of variance explained by the k^{th} PC averaged for all state matrices. As PCs can have arbitrary directions, negative absolute Pearson's correlation was utilized as the distance function.

c) Stacked Spatiotemporal Slices (S-STS): An alternative embedding strategy was based on flattening individual state matrices (shown in (4)) into column vectors using column-major order and stacking them into a grand state matrix, $\hat{S}$:

$$\hat{S} = [S_1^{'}, S_2^{'}, ..., S_L^{'}]^T, \quad (8)$$

with $S_i^{'}$ the flattened version of state matrix S_i. Applying SVD on $\hat{S}$ (as in (6)) yielded the principal spatiotemporal slices and their variations over time. This variation information was contained in the columns of U matrix $(u_1, u_2, ..., u_L)$. Then, signal can be represented based on the first M columns of matrix U for time point i:

$$\vec{x}(i) = [u_1(i), u_2(i), ..., u_M(i)], \quad (9)$$

which was used to detect distances in the subsequent stage as $D_{i,j} = ||\vec{x}(i) - \vec{x}(j)||_2$.

C. Detection of Repetitive Patterns with Recurrence Plots

Repetitive pattern detection framework started with extracting spatiotemporal slices for each time point from atrial electrograms (blue and red stripes in Fig. 1A). Consequently, distances between slices were computed based on the approaches summarized in section II-B in order to form a distance matrix (Fig. 1B)). Thresholding the computed distance matrix yielded the RP shown in Fig. 1C.

Constructed RPs were analyzed to detect repetitive intervals as in [5]. Briefly, a repetitive pattern that is repeatedly observed for several consecutive AF cycles will form a square block on the main diagonal of the RP, filled with

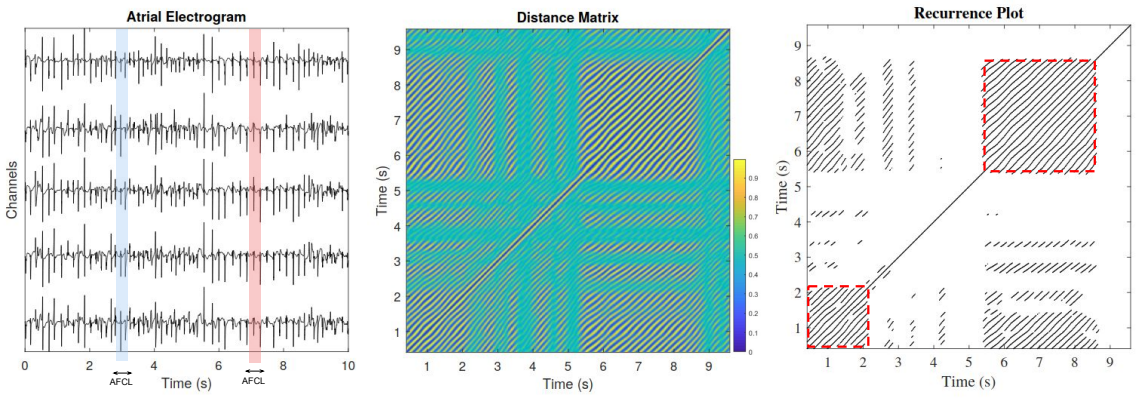

Fig. 1. (A) Atrial electrogram with S_i (blue) and S_j (red), two AFCL-sized spatiotemporal slices, (B) Distance plot containing distances between all pairs of spatiotemporal slices using FD-STS, (C) Recurrence plot (RP) generated by thresholding the distance matrix together with detected repetitive intervals (square-shape regions on the diagonal of the RP).

diagonal lines with a recurrence rate that corresponds (approximately) to one recurrence per AF cycle. To find these blocks an algorithm determined the largest block with at least this recurrence rate at every position on the main diagonal of the RP. Local maxima of the duration of these blocks were defined as intervals containing repetitive patterns (see Fig. (1C)). Based on this timing information, we calculated:

- Repetitive interval detection sensitivity and specificity of each method compared to the reference technique.
- Repetitive pattern prevalence (percentage of recording duration that is occupied by repetitive patterns).

RPs together with the repetitive intervals they contained were extracted using the tool proposed in [5] and were used as references. RPs generated using different approaches were compared with these references by means of three measures: (i) DICE coefficient (twice the number of elements common to both sets divided by the sum of the number of elements in each set) which quantifies the pixel-to-pixel similarity taking values between 0 (no correspondence) to 1 (perfect correspondence), (ii) Sensitivity (percentage of true positives) to repetitive patterns and (iii) specificity (percentage of true negatives). Differences between different methods were analyzed with the Kruskal-Wallis non-parametric test with Conover squared ranks test to account for multiple comparisons.

For all proposed techniques, RPs were constructed using an adaptive AF cycle recurrence rate-based threshold ε (c.f. [5]). Hyperparameters such as the number of PCs used in PCA-STS and S-STS were chosen such that the DICE coefficients were maximized on an independent training dataset of 12 patients which was excluded from the analyses.

III. RESULTS

Multiple comparisons between approaches and conditions (pAF and persAF) were performed (see Table I). Although all approaches showed reductions in average DICE coefficients and sensitivity among pAF and persAF conditions, these were not found significant ($p > 0.01$). This reflects stability of these approaches against increasing disease complexity.

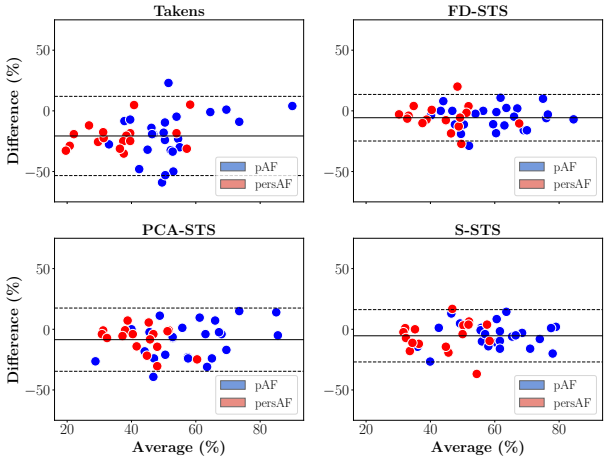

Fig. 2. Bland-Altman Plots for prevalence of repetitive patterns. Solid lines represents the mean percentage differences while dashed lines indicates the confidence intervals.

STS approaches achieved significantly higher DICE coefficients and sensitivities than Takens' approach while significant differences among STS methods were not observed. No significant effect was found for specificity values.

Average prevalence over all recordings obtained by each method and the reference were summarized in Table II. All approaches detected significantly lower prevalence values compared to the reference in both pAF and persAF patients. These results suggested that the proposed techniques underestimated the reference prevalence values.

To reveal each model's response to varying prevalence, Bland-Altman plots were constructed (see Fig. (2)). Each plot was method-specific and exhibited the relation of average prevalence detected by that method (x-axis) and the reference against their difference (y-axis). These plots visually verified: (i) Weaker performance of Takens approach as points were more distributed in $y-$axis, (ii) persAF samples (red points) were more dense for lesser values on $x-$axis suggesting the lower prevalence values in persistent types of AF, (iii) increased proportional bias of Takens' approach

TABLE I

DICE COEFFICIENTS AND SENSITIVITY/SPECIFICITY VALUES FOR EACH METHOD.

Methods	pAF			persAF		
	DICE	Sensitivity	Specificity	DICE	Sensitivity	Specificity
Takens	49.23±14.36	58.49±23.21	73.43±17.21	42.69±5.96	47.91±20.06	82.11±13.49
FD-STS	82.39±7.21	87.36±13.64	87.17±11.21	77.77±10.34	82.73±12.76	79.61±16.03
PCA-STS	81.86±11.87	82.48±16.61	85.57±12.40	80.66±6.71	76.82±16.46	87.53±13.55
S-STS	87.87±9.32	86.84±10.59	87.53±12.47	81.76±8.10	81.04±12.29	85.22±12.31

TABLE II

MEAN DETECTED PREVALENCE AND REGRESSION COEFFICIENTS FOR BLAND-ALTMAN PLOTS

Methods	Mean Prevalence (%)		Regression Coefficients	
	pAF	persAF	pAF	persAF
Reference	61.42	45.89	-	-
Takens	44.63	28.13	1.25(*)	1.29(*)
FD-STS	57.42	41.38	1.24	-0.11
PCA-STS	56.74	40.26	0.86	1.14
S-STS	59.39	41.04	0.94	0.40

(*) $p < 0.01$

as points were left-skewed. Lastly, Bland-Altman plots were analyzed to reveal linear relationships between average and difference prevalence values detected by different techniques. This information was acquired by fitting a linear model to individual methods' plots by ordinary least squares method. As shown in Table II, Takens' approach was the only method with statistically significant linear relation in both pAF and persAF patients. The regression was positive suggesting a convergence to zero difference in prevalence while average prevalence was increasing. In other words, performance of Takens' in estimating prevalence was improved for recordings with larger prevalence. In contrast, STS approaches did not show any average prevalence-dependent behavior as no significant linear relation was found.

IV. DISCUSSION

Different electrogram embedding approaches were able to detect repetitive spatiotemporal patterns during AF with various degrees of accuracy. The conventional Takens approach had substantially lower DICE coefficients (pAF=49.23, persAF=42.69) and sensitivities (pAF=58.49, persAF=47.91). Takens approach depends on the False Nearest Neighbour and Average Mutual Information for embedding parameter configuration. This was contrasted by STS approaches which defined each atrial conduction state as an AFCL-sized spatiotemporal slice. Our results exhibited the efficacy of using $a\ priori$ knowledge, such as AFCL during embedding.

STS-based methods achieved promising results on replicating the RPs achieved by the reference technique. The differences among STS techniques (in DICE, sensitivity and specificity) were not significant. While FD-STS utilized all signal amplitude information with the spatiotemporal slices, PCA-STS operated on a few first PCs extracted from electrograms. This brought multiple advantages: (i) reduction in spatial redundancy, (ii) relaxing the electrode-electrode correspondence during distance calculations by projecting the data on its principal axes. The latter property enables the usage of PCA-STS in applications where electrode positions are not stable during the recordings. It was observed that reorganization of spatiotemporal slices and applying PCA on this matrix, as in S-STS, was also effective. This approach is equivalent to implicitly vectorized PCA on 3-mode tensors formed by stacking spatiotemporal slices on the third dimension of a tensor and may potentially be more efficiently executed using tensor decomposition techniques [8].

Prevalence of repetitive patterns is a feature that may be associated with the underlying complexity of wave propagation during AF. Patients with persAF were expected to have fewer, shorter lasting repetitive patterns and consequently smaller prevalence. All proposed approaches were able to capture this characteristic. Moreover, as no linear trend was visible in Bland-Altman plots for STS methods, we conclude that STS approaches are equally sensitive to recordings with low and high prevalence of repetitive patterns, making them robust tools for extraction of repetitiveness-based features.

REFERENCES

[1] Oral, H., Knight, B. P., Tada, H., Ozaydin, M., Chugh, A., Hassan, S., Morady, F. (2002). Pulmonary vein isolation for paroxysmal and persistent atrial fibrillation. Circulation, 105(9), 1077-1081.

[2] Lee, S., Sahadevan, J., Khrestian, C. M., Cakulev, I., Markowitz, A., & Waldo, A. L. (2015). Simultaneous biatrial high-density (510–512 electrodes) epicardial mapping of persistent and long-standing persistent atrial fibrillation in patients: new insights into the mechanism of its maintenance. Circulation, 132(22), 2108-2117.

[3] Jalife, J. (2011). Deja vu in the theories of atrial fibrillation dynamics. Cardiovascular research, 89(4), 766-775.

[4] Eckmann, J. P., Kamphorst, S. O., & Ruelle, D. (1995). Recurrence plots of dynamical systems. World Scientific Series on Nonlinear Science Series A, 16, 441-446.

[5] Zeemering, S., Van Hunnik, A., Van Rosmalen, F., Bonizzi, P., Scaf, B., Delhaas, T., ... & Schotten, U. (2020). A Novel Tool for the Identification and Characterization of Repetitive Patterns in High-Density Contact Mapping of Atrial Fibrillation. Frontiers in physiology, 11, 1304.

[6] Botteron, G. W., & Smith, J. M. (1995). A technique for measurement of the extent of spatial organization of atrial activation during atrial fibrillation in the intact human heart. IEEE transactions on biomedical engineering, 42(6), 579–586. https://doi.org/10.1109/10.387197

[7] Kantz, H., & Schreiber, T. (2004). Nonlinear time series analysis (Vol. 7). Cambridge university press.

[8] Zare, A., Ozdemir, A., Iwen, M. A., & Aviyente, S. (2018). Extension of PCA to higher order data structures: An introduction to tensors, tensor decompositions, and tensor PCA. Proceedings of the IEEE, 106(8), 1341-1358.